Inorg. Chem. **2004**, *43*, 4026–4035

Investigation of the Incommensurate and Commensurate Magnetic Superstructures of $LiCuVO_4$ and CuO on the Basis of the Isotropic Spin Exchange and Classical Spin Approximations

D. Dai, H.-J. Koo, and M.-H. Whangbo*

Department of Chemistry, North Carolina State University, Raleigh, North Carolina 27695-8204

Received November 13, 2003

The spin lattices of magnetic oxides $LiCuVO_4$ and CuO are made up of CuO_2 ribbon chains. The incommensurate and commensurate magnetic superstructures of these oxides were examined by calculating the total spin exchange interaction energies of their long-range order spin arrangements on the basis of the isotropic spin exchange and classical spin approximations. The incommensurate superstructure (0, 0.532, 0) of $LiCuVO_4$ was analyzed to find that the next-nearest-neighbor spin exchange interaction J_{nnn} is more strongly antiferromagnetic than the nearest-neighbor spin exchange interaction J_{nn} in the CuO_2 chains. With this finding, we reassessed the relative strengths of the spin exchange interactions of $LiCuVO_4$ and CuO and then analyzed the relative energies of their long-range order spin arrangements. The incommensurate superstructure (0, 0.532, 0) of $LiCuVO_4$ is explained when the J_{nn}/J_{nnn} ratio is −0.40. Both the incommensurate superstructure (0.506, 0, −0.483) and the commensurate superstructure (0.5, 0, −0.5) of CuO, which occur at 231 and 212.5 K, respectively, are well explained in terms of the calculated total spin exchange interaction energies. The incommensurate superstructure of CuO becomes commensurate by a slight change in one interchain spin exchange interaction, which is due probably to a slight structure change brought about by the temperature lowering.

1. Introduction

As building blocks of their magnetic lattices, a number of magnetic oxides have CuO_2 ribbon chains containing spin-$^1/_2$ Cu^{2+} ions (Figure 1a). For instance, $LiCuVO_4$ [1] and Li_2CuO_2 [2] have isolated CuO_2 ribbon chains while CuO,[3] Cu_4O_3, [4] and $Ag_2Cu_2O_3$ [5] have CuO_2 ribbon chains condensed by oxygen corner-sharing. Upon lowering the temperature, some of these oxides undergo a long-range order (LRO) spin ordering which leads to magnetic superstructures.[6−8] The physical and structural properties of magnetic solids are commonly described by considering their spin exchange interactions. For an isolated CuO_2 ribbon chain, the spin exchange interactions of interest are the nearest-neighbor (NN) interaction J_{nn}, which takes place through the two Cu−O−Cu superexchange (SE) paths, and the next-nearest-neighbor (NNN) interaction J_{nnn}, which takes place through

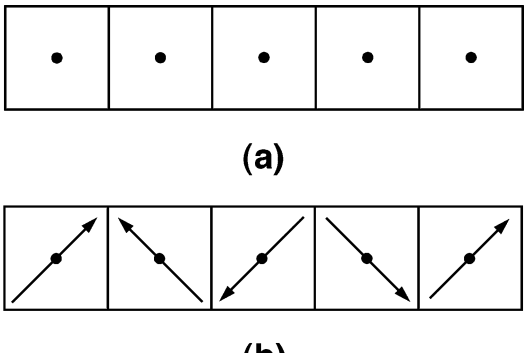

Figure 1. (a) Schematic view of a CuO_2 ribbon chain made up of edge-sharing CuO_4 square planes, where the dots represent the Cu^{2+} ions. (b) LRO spin arrangement of the CuO_2 ribbon chains in the magnetic superstructure (0, 0.532, 0) of $LiCuVO_4$.

* To whom correspondence should be addressed. E-mail: mike_whangbo@ncsu.edu.

(1) (a) Lafontaine, M. A.; Leblanc, M.; Ferey, G. *Acta Crystallogr., Sect. C* **1989**, *45*, 1205. (b) Kanno, R.; Kawamoto, Y.; Takeda, Y.; Hasegawa, M.; Yamamoto, O.; Kinimura, N. *J. Solid State Chem.* **1992**, *96*, 397.
(2) Sapiña, F.; Rodríguez-Carvajal, J.; Sanchis, M. J.; Ibáñez, R.; Beltrán, A.; Beltrán, D. *Solid State Commun.* **1990**, *74*, 779.
(3) Åsbrink, S.; Norrby, L.-J. *Acta Crystallogr., Sect. B* **1970**, *26*, 8.
(4) O'Keeffe, M.; Bovin, J.-O. *Am. Mineral.* **1978**, *63*, 180.
(5) (a) Gómez-Romero, P.; Tejada-Rosales, E. M.; Palacín, M. R. *Angew. Chem., Int. Ed.* **1999**, *38*, 524. (b) Tejada-Rosales, E.; Rodríguez-Carvajal, J.; Casañ-Pastor, N.; Alemany, P.; Ruiz, E.; El-Fallah, M. S.; Alvarez, S.; Gómez-Romero, P. *Inorg. Chem.* **2002**, *41*, 6604.
(6) Gibson, B. J.; Kremer, R. K.; Prokofiev, A. V.; Assmus, W.; McIntyre, G. J. *Physica B*, in press.

10.1021/ic035314c CCC: $27.50
Published on Web 05/28/2004

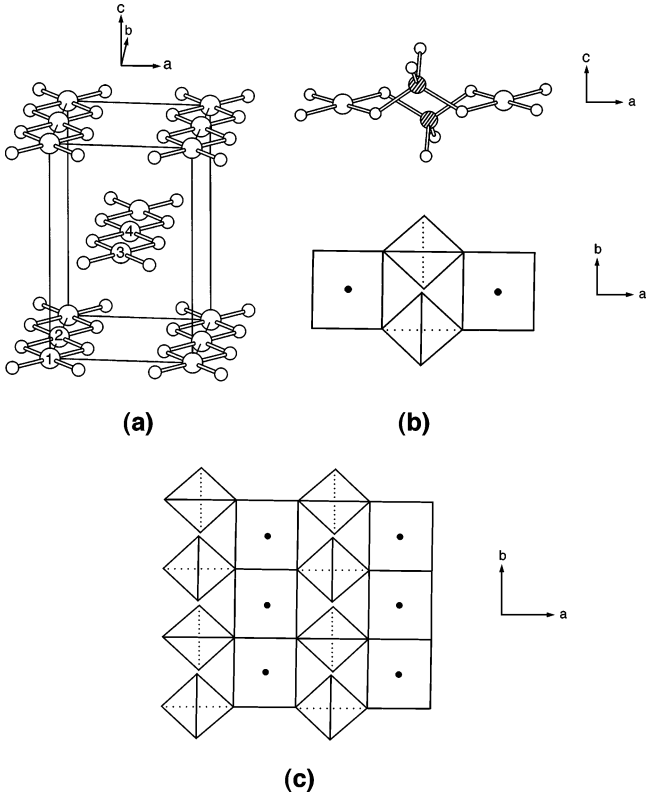

Figure 2. (a) Arrangement of the CuO_2 chains in $LiCuVO_4$ (Cu = larger circles, O = smaller circles). (b) Perspective (top) and schematic projection (bottom) views of how CuO_4 square planes are condensed with VO_4 tetrahedra (V = shaded circles). (c) Extended projection view showing how CuO_2 chains are linked by VO_4 tetrahedra to form a $CuVO_4$ layer parallel to the *ab*-plane. The Li^+ ions are located between the $CuVO_4$ layers.

the two Cu−O···O−Cu super-superexchange (SSE) paths. The interchain NN spin exchange interactions of these magnetic oxides are either SE or SSE interactions depending on how their CuO_2 chains are arranged in the crystal lattice.

In $LiCuVO_4$, the CuO_2 chains are aligned along the crystallographic *b*-direction (Figure 2),[1] and each CuO_2 chain has two Cu^{2+} ions per chemical unit cell. The magnetic susceptibility[9] of $LiCuVO_4$ exhibits a broad maximum at T_M = 28 K and is described by a Heisenberg antiferromagnetic chain model with spin exchange parameter of −45 K (under the convention in which each pairwise spin exchange interaction is written as $-J_{ij}\hat{\mathbf{S}}_i\cdot\hat{\mathbf{S}}_j$ instead of $-2J_{ij}\hat{\mathbf{S}}_i\cdot\hat{\mathbf{S}}_j$). A recent neutron diffraction study[6] established that $LiCuVO_4$ forms an incommensurate magnetic superstructure (0, 0.532, 0) below 2.1 K, which is equivalent to (0, 0.468, 0). This superstructure is close to the commensurate one (0, 0.5, 0). In this commensurate approximation, each CuO_2 chain in the magnetic superstructure of $LiCuVO_4$ contains four Cu^{2+} ions per magnetic unit cell, and the associated spin arrangement (Figure 1b) shows that the NNN spins are antiferromagnetically coupled, while the NN spins are oriented nearly orthogonal to each other.[6] This means that the antiferromagnetic NNN spin exchange interaction J_{nnn} (<0) is much stronger in magnitude than the NN spin exchange interaction J_{nn} (either ferromagnetic or antiferromagnetic), i.e., $|J_{nn}| \ll |J_{nnn}|$. Consequently, the intrachain spin exchange parameter of −45 K, deduced from the magnetic susceptibility of $LiCuVO_4$, must refer to the NNN spin exchange J_{nnn}, not to the NN spin exchange J_{nn}. Indeed, this conclusion has recently been verified by Kremer,[10] who fitted the magnetic susceptibility of $LiCuVO_4$ using the high-temperature series expansion formula of Bühler et al.[11] The interchain spin exchange of $LiCuVO_4$ is found to be much weaker than the intrachain spin exchange,[9] so that the occurrence of the magnetic superstructure in $LiCuVO_4$ must largely be driven by the tendency for each CuO_2 chain to have its NNN spins order antiferromagnetically.

In the three-dimensional lattice of cupric oxide CuO,[3] all oxygen atoms participate in corner-sharing between adjacent CuO_2 chains, and every two CuO_2 chains condensed by oxygen corner-sharing are not perpendicular to each other (see below). CuO exhibits an incommensurate antiferromagnetic superstructure (0.506, 0, −0.483) below T_{N1} = 231 K, which becomes a commensurate antiferromagnetic superstructure (0.5, 0, −0.5) below T_{N2} = 212.5 K.[7b] In Cu_4O_3[4] and $Ag_2Cu_2O_3$,[5] the CuO_2 ribbon chains form the Cu_2O_3 lattice by oxygen corner-sharing, and the Cu^{2+} ions of this lattice form a pyrochlore spin lattice, an archetypal geometrically frustrated spin lattice.[12] Nevertheless, Cu_4O_3 was found to undergo an LRO spin arrangement below 42.3 K to form a magnetic superstructure (0.5, 0.5, 0.5).[8] To understand such incommensurate and commensurate magnetic superstructures of transition metal magnetic oxides, it is necessary to know the signs and the relative strengths of the spin exchange interactions associated with various spin exchange paths. For this purpose, either first principles or qualitative electronic structure calculations are carried out for various spin dimers (i.e., structural units containing two spin sites) of a magnetic solid under consideration.[13,14] In the qualitative analysis based on extended Hückel tight binding (EHTB) calculations,[15] the relative strengths of SE and SSE interactions of transition metal oxides depend sensitively on the diffuseness of the oxygen 2p orbital.[14,16] Thus, there arise occasions requiring the calibration of calculated results on the basis of appropriate experimental results. In the previous studies of Cu_4O_3[16] and CuO,[17] their spin exchange parameters were calibrated using the assign-

(7) (a) Forsyth, J. B.; Brown, P. J.; Wanklyn, B. M. *J. Phys. C: Solid State Phys.* **1988**, *21*, 2917. (b) Yang, B. X.; Thurston, T. R.; Tranquada, J. M.; Shirane, G. *Phys. Rev. B* **1989**, *39*, 4343.
(8) (a) Elhajal, M.; Canals, B.; Lacroix, C. *J. Phys.: Condens. Matter* **2004**, *16*, 2004. (b) Pinsard-Gaudart, J.; Rodríguez-Carvajal, J.; Gukasov, A.; Monod, P.; Dechamps, M.; Jegoudez, J. Propriétés magnétiques de Cu_4O_3-Un reseau pyrochlore à spin 1/2. Presented at Colloque Oxydes à Propriétés Remarquables: Ordre de spins, ordre de charges et phénomènes coopératifs, Bombannes, France, June 6−8, 2001; organized by Berthier, C., Collin, G., Doumerc, J.-P. The abstracts of the meeting are collected in the report GDR 2069.
(9) Vasil'ev, A. N.; Ponomarenko, L. A.; Manaka, H.; Yamada, I.; Isobe, M.; Ueda, Y. *Physica B* **2000**, *284−286*, 1619.
(10) Kremer, R. K. Private communication.
(11) Bühler, A.; Elstner, N.; Uhrig, G. S. *Eur. Phys. J. B* **2000**, *16*, 475.
(12) Greedan, J. E. *J. Mater. Chem.* **2001**, *11*, 37.
(13) Illas, F.; Moreira, I. de P. R.; de Graaf, C.; Barone, V. *Theor. Chem. Acc.* **2000**, *104*, 265 and references therein.
(14) For a recent review, see: Whangbo, M.-H.; Koo, H.-J.; Dai, D. *J. Solid State Chem.* **2003**, *176*, 417.
(15) Hoffmann, R. *J. Chem. Phys.* **1963**, *39*, 1397.
(16) Whangbo, M.-H.; Koo, H.-J. *Inorg. Chem.* **2002**, *41*, 3570.
(17) Koo, H.-J.; Whangbo, M.-H. *Inorg. Chem.* **2003**, *42*, 1187.

ment of $J_{nn} = -45$ K for $LiCuVO_4$, which is incorrect according to the recent neutron diffraction study[6] as pointed out above. Thus, the spin exchange parameters of these oxides should be reassessed using the correct assignment $J_{nnn} = -45$ K for $LiCuVO_4$.

In predicting what LRO spin arrangement is energetically favorable for a given magnetic solid, it is necessary to calculate its total spin exchange interaction energies for all possible incommensurate and commensurate LRO spin arrangements. For a magnetic solid whose spins are coupled by isotropic spin exchange interactions, this can be achieved by employing the classical spin and the internal field approximations as described by Freiser more than four decades ago (hereafter the Freiser method, see section 4).[18] Given a set of spin exchange parameters assigned to a magnetic solid, this method determines what LRO spin arrangement leads to the lowest total spin exchange energy state. Consequently, the Freiser method may be used to test whether the assigned set of spin exchange parameters is consistent with its LRO magnetic superstructure and what set of spin exchange parameters is required to explain the observed magnetic superstructure. Recently, the Freiser method has been employed to interpret the magnetic structures of $LiFeP_2O_7$,[19,20] $NaFeP_2O_7$,[20] and $Fe_2(SO_4)_3$.[21]

In the present work, we use the Freiser method to gain insight into what electronic factor is responsible for the formation of the incommensurate magnetic superstructures in $LiCuVO_4$ and CuO as well as for the conversion of the incommensurate structure of CuO to the commensurate one that a slight temperature lowering brings about. Our analysis of the commensurate superstructure of Cu_4O_3 will be reported later. The present work is organized as follows: in section 2 we briefly describe the crystal structures of $LiCuVO_4$ and CuO to specify their spin exchange paths. In section 3, we estimate the relative strengths of the spin exchange parameters of $LiCuVO_4$ and CuO on the basis of spin dimer analysis. The essence of the Freiser method is summarized in section 4. The origin of the incommensurate superstructure of $LiCuVO_4$ is discussed in section 5. We analyze the incommensurate and commensurate superstructures of CuO in section 6. Implications of our results presented in sections 5 and 6 are discussed in section 7. Important findings of our work are summarized in section 8.

2. Spin Dimers of $LiCuVO_4$ and CuO

The arrangement of the CuO_2 chains in $LiCuVO_4$ is shown in Figure 2a. There are four Cu^{2+} ions in a unit cell as indicated in Figure 2a. The spin exchange paths to consider for $LiCuVO_4$ are J_{nn}, J_{nnn}, and the interchain interaction J_a along the *a*-direction (Table 1). The interchain interactions along the $(a + c)$- and *c*-directions should be much weaker than that along the *a*-direction, because the CuO_4 square planes containing their magnetic orbitals (i.e., the singly occupied molecular orbitals) are coplanar only for those interactions along the *a*-direction.[14] It is noted that the J_{nnn} and J_a interactions are both SSE interactions. The spin dimer representing the J_{nn} interaction is given by the Cu_2O_6 cluster (Figure 3a), and that representing the J_{nnn} and J_a interactions by the Cu_2O_8 cluster (Figure 3b). In $LiCuVO_4$, the adjacent CuO_2 chains contained in the *ab*-plane condense with VO_4 tetrahedra, as depicted in Figure 2b, to form a $CuVO_4$ layer (Figure 2c), and the Li^+ ions are located between the $CuVO_4$ layers.

Table 1. Cu···Cu Distances and Relative Strengths of the Spin Exchange Parameters of $LiCuVO_4$

path	nature	Cu···Cu (Å)	$-(\Delta e)^2$ [(meV)^2]	J_{AF}/k_B
J_{nn}	SE	2.899	−530	−3.4
J_{nnn}	SSE	5.799	−7060	−45
J_a	SSE	5.652	−4700 (−110)[a]	−30 (−0.7)[a]

[a] The numbers in parentheses were obtained using the spin dimers containing the VO_4 tetrahedra (see the text).

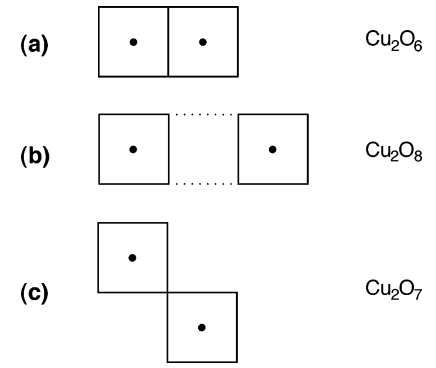

Figure 3. Three types of spin dimers in the oxides made up of CuO_2 chains: (a) spin dimer Cu_2O_6 for an intrachain SE interaction, (b) spin dimer Cu_2O_8 for an interchain SSE interaction, (c) spin dimer Cu_2O_7 for an interchain SE interaction.

Note that the SSE interactions J_{nnn} and J_a become qualitatively different once the effect of the VO_4 tetrahedra is taken into consideration. In the spin dimer representing the J_a interaction, the two oxygen atoms of each Cu−O··· O−Cu exchange path form an O−V−O bridge (Figure 4a). This is not the case in the spin dimer representing the J_{nnn} interaction (Figure 4b). As will be discussed in the next section, this difference between the J_{nnn} and J_a has a profound consequence on the relative strengths of their spin exchange interactions.

The atoms of a unit cell in CuO are shown in Figure 5a, and the arrangement of the CuO_2 ribbon chains in CuO is shown in Figure 5b. There are four Cu^{2+} ions in a unit cell, and their positions are indicated in Figure 5a and are listed in Table 2a. The spin exchange paths to consider for CuO are J_{nn}, J_{nnn}, and the interchain interactions J_1, J_2, and J_3 defined in Table 2b with the help of Figure 5c. Here, all the interchain interactions are SE interactions, and the spin dimers representing them are given by the Cu_2O_7 clusters (Figure 3c). As can be seen from Figure 5c, the SE paths of CuO give rise to several different magnetic chains, i.e., $[Cu(a)-O-Cu(\kappa)-O]_\infty$ (κ = b, c, d, e) chains.[17]

(18) Freiser, M. J. *Phys. Rev.* **1961**, *123*, 2003.
(19) Rousse, G.; Rodríguez-Carvajal, J.; Wurm, C.; Masquelier, C. *Solid State Sci.* **2002**, *4*, 973.
(20) Whangbo, M.-H.; Dai, D.; Koo, H.-J. *Dalton Trans.*, in press.
(21) Dai, D.; Whangbo, M.-H.; Koo, H.-J. *Inorg. Chem.*, submitted for publication.

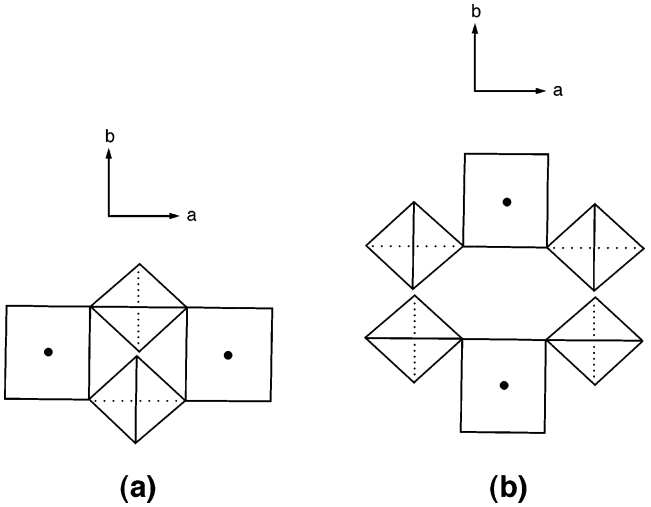

Figure 4. Two different SSE paths of $LiCuVO_4$: (a) interchain interaction with the SSE paths bridged by VO_4 tetrahedra, (b) intrachain interaction with the SSE paths not bridged by VO_4 tetrahedra.

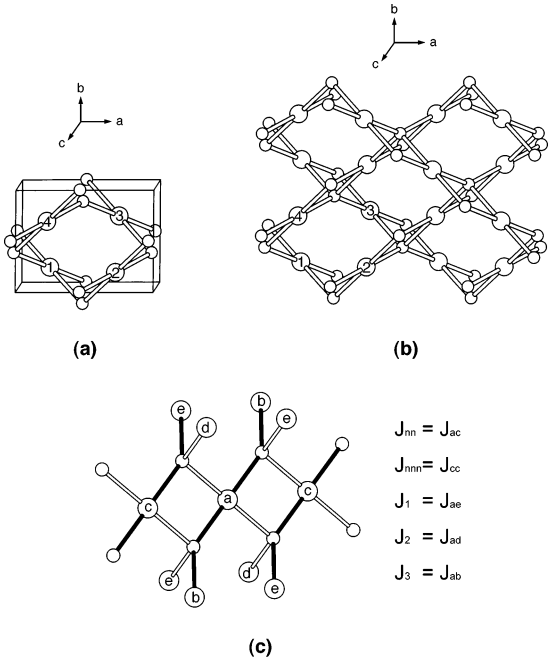

Figure 5. (a) Atoms of a unit cell in CuO. (b) Arrangement of CuO_2 chains in CuO. (c) Arrangement of several Cu^{2+} ions surrounding one Cu^{2+} ion in CuO (Cu = larger circles, O = smaller circles). The Cu atoms labeled a−e are used to define the spin exchange paths in Table 2b.

3. Spin Exchange Interactions of $LiCuVO_4$ and CuO

In general, a spin exchange parameter J is written as $J = J_F + J_{AF}$, where the ferromagnetic term J_F (> 0) is small, so that the spin exchange becomes ferromagnetic (i.e., $J > 0$) when the antiferromagnetic term J_{AF} (<0) is negligibly small in magnitude. Spin exchange interactions of magnetic solids are mostly antiferromagnetic (i.e., $J < 0$), and can be discussed by focusing on the antiferromagnetic terms J_{AF}.[14] If each spin site of a magnetic solid contains one unpaired electron and if the two spin sites of a spin dimer are equivalent, then the antiferromagnetic term J_{AF} is written as[14]

$$J_{AF} = -(\Delta e)^2/U_{eff} \qquad (1)$$

Table 2. Cu Atom Positions and Spin Exchange Parameters of CuO

(a) Fractional Coordinates of the Cu Atoms in a Unit Cell

	x	*y*	*z*
Cu1	0.25	0.25	0
Cu2	0.75	0.25	0.5
Cu3	0.75	0.75	0
Cu4	0.25	0.75	0.5

(b) Cu···Cu Distances and Relative Strengths of Spin Exchange Paths

path	nature	Cu···Cu (Å)	$-(\Delta e)^2$ [(meV)^2]	J_{AF}/k_B
J_{nn}	SE	2.901 (a···c)[a]	−441	−2.8
J_{nnn}	SSE	5.801 (c···c)[a]	−7160	−45
J_1	SE	3.083 (a···e)[a]	−7230	−46
J_2	SE	3.173 (a···d)[a]	−8650	−55
J_3	SE	3.749 (a···b)[a]	−137000	−870

[a] The labels a−e in the parentheses refer to the Cu atoms defined in Figure 5c.

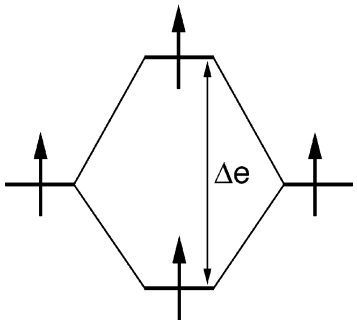

Figure 6. Spin−orbital interaction energy Δe between the two magnetic orbitals representing the two spin sites of a spin dimer.

where Δe is the spin−orbital interaction energy (Figure 6) between two magnetic orbitals representing the two spin sites, and U_{eff} is the effective on-site repulsion. For a set of closely related magnetic solids, the U_{eff} value is nearly constant so that the trend in J_{AF} is well approximated by that in the corresponding $-(\Delta e)^2$.[14]

In describing the spin exchange interactions of magnetic solids in terms of Δe values obtained from EHTB calculations, it is found[14] necessary to employ double-ζ Slater type orbitals (STOs)[22] for both the d orbitals of the transition metal and the s/p orbitals of the surrounding ligand atoms. The atomic orbital parameters of Cu and O employed for our calculations were described in the previous study on Cu_4O_3.[16] The radial part of the O 2p orbital, $\chi_{2p}(r)$, is written as

$$\chi_{2p}(r) = r[C \exp(-\zeta r) + C' \exp(-\zeta' r)] \qquad (2)$$

where $\zeta > \zeta'$. The $(\Delta e)^2$ values depend most sensitively on the value of the diffuse exponent ζ' according to the previous study,[16] which examined how the $(\Delta e)^2$ values vary as the ζ' value is gradually increased as $\zeta'(x) = 1.659(1 + x)$, i.e., as the diffuseness of the O 2p orbital tail is gradually decreased ($x \geq 0$). Here, the $\zeta'(0)$ value represents the value taken from the STOs tabulated by Clementi and Roetti.[22] The assignment of $J_{nn} = -45$ K in $LiCuVO_4$ required the use of a more contracted $\zeta'(x)$ value, i.e., $\zeta'(0.125)$, for the calculation of $(\Delta e)^2$.[16] However, as discussed in section 1, $J_{nnn} = -45$ K and $|J_{nn}| \ll |J_{nnn}|$ in $LiCuVO_4$. The latter is

(22) Clementi, E.; Roetti, C. *At. Data Nucl. Data Tables* **1974**, *14*, 177.

reproduced by a more diffuse $\zeta'(x)$ value, i.e., $\zeta'(0)$. Thus, for the various spin exchange paths of $LiCuVO_4$ and CuO, we recalculate their $(\Delta e)^2$ values using the $\zeta'(0)$ value on the basis of the spin dimers representing the spin exchange paths (Figure 3).[23] Our results are summarized in Tables 1 and 2b for $LiCuVO_4$ and CuO, respectively. The spin exchange parameters obtained from $\zeta'(0)$ show that $J_{nnn} < 0$ and $J_{nn} \approx 0$, while the reverse was the case in terms of those obtained from $\zeta'(0.125)$. The parameters calculated with both $\zeta'(0.125)$ and $\zeta'(0)$ show that the dominant antiferromagnetic interaction of CuO is the interchain SE interaction J_3. However, the J_3 interaction is more strongly antiferromagnetic with the use of $\zeta'(0)$.

To determine the LRO magnetic superstructure expected for $LiCuVO_4$ and CuO using the Freiser method, rough estimates of the relative strengths of their spin exchange parameters are needed. For this purpose, we convert the calculated $(\Delta e)^2$ values into the corresponding spin exchange parameters by scaling them linearly in such a way that the $-(\Delta e)^2$ value for the intrachain NNN spin exchange path J_{nnn} of $LiCuVO_4$ becomes -45 K. The resulting parameters are listed in Tables 1 and 2b. In employing these parameters, it should be recalled that a spin exchange parameter J consists of two terms, i.e., $J = J_F + J_{AF}$, but our estimation ignored the ferromagnetic term J_F. For a given spin dimer whose spin sites are described by two magnetic orbitals ϕ_1 and ϕ_2, the J_F term is equal to $2K_{12}$, where K_{12} is the exchange repulsion integral between ϕ_1 and ϕ_2. The K_{12} value can be non-negligible if the p-orbital tails of the magnetic orbitals ϕ_1 and ϕ_2 are located on a same ligand atom, but it becomes negligible otherwise.[14,24] Thus, the effect of the J_F term is more important for SE interactions than for SSE interactions (see section 6 for further discussion).

It is noted from Table 1 for $LiCuVO_4$ that when the $(\Delta e)^2$ values of the SSE interactions are calculated using the spin dimers Cu_2O_8 (Figure 3b), the interchain NN interaction J_a is only slightly weaker than the intrachain NNN interaction J_{nnn}, in disagreement with experiment.[9] This failure results from neglecting the fact that the VO_4 units affect the SSE interactions J_a and J_{nnn} differently. The Δe for an SSE interaction is the energy difference between the bonding level ψ_+ and the antibonding level ψ_- (Figure 7a) of the spin dimer. In the path J_a, the empty d orbital of the V atom forming the O−V−O bridge with the oxygen atoms of the Cu−O···O−Cu path (Figure 4a) interacts in-phase with both O 2p orbital tails of the antibonding level ψ_- (Figure 7b), thereby lowering the ψ_- level. However, by symmetry, this effect does not occur for the bonding level ψ_+. Consequently, the interaction energy Δe is reduced. Such a preferential reduction of the interaction energy Δe does not occur in the case of the exchange path J_{nnn}, because the oxygen atoms of each Cu−O···O−Cu path do not form an O−V−O bridge (Figure 4b). Our calculations of the $(\Delta e)^2$ values using the spin dimers including two VO_4 tetrahdra, presented in Figure 4a,b, show a significant reduction of the Δe value for the path J_a, but not for the path J_{nnn}. The $(\Delta e)^2$ value for J_a estimated by including the effect of the VO_4 tetrahedra, shown in parentheses, is negligible compared with that for J_{nnn}. The latter is consistent with the observed magnetic superstructure (0, 0.532, 0) of $LiCuVO_4$,[6] which shows that the interchain SSE interactions along the *a*- and *c*-directions are ferromagnetic.

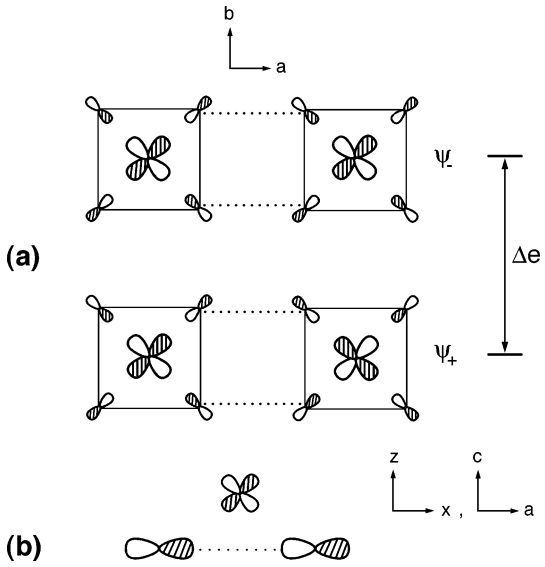

Figure 7. (a) Bonding and antibonding levels, ψ_+ and ψ_-, respectively, of a spin dimer Cu_2O_8 representing an SSE interaction. (b) Energy-lowering effect of the V d_{xz} level on the antibonding level ψ_- in the interchain SSE path J' of $LiCuVO_4$. The V d_{xz} orbital makes a bonding interaction with both O 2p orbital tails of ψ_- in the Cu−O···O−Cu paths.

4. Classical Spin Analysis of Magnetic Superstructures

The Freiser method[18] assumes that spins can adopt all possible directions in space (the classical spin approximation), the orientational distributions of the spins are independent, and the spin exchange interactions are isotropic. Suppose that a magnetic solid is in an LRO magnetic state *i*, in which the spin sites μ (=1, 2, ..., *m*) of the unit cell located at the coordinate origin (i.e., the lattice vector $\mathbf{R} = 0$) have the mean spins σ_μ^0. At high temperatures, the spins are completely disordered so that $\sigma_\mu^0 = 0$ for all $\mu = 1, 2, ..., m$. As the temperature is lowered, an ordered spin state may set in thereby leading to nonzero σ_μ^0.

For a magnetic solid with repeat vectors **a**, **b**, and **c**, the ordered spin arrangement can be described in terms of the "Bloch" spin functions $\sigma_\mu(\mathbf{k})$

$$\sigma_\mu(\mathbf{k}) = \frac{1}{\sqrt{N}} \sum_R \sigma_\mu^0 \exp(i\mathbf{k}\cdot\mathbf{R}) \qquad (3)$$

where *N* is the number of unit cells in the magnetic solid and **k** is the wave vector. The lattice vector **R** is written as

$$\mathbf{R} = n_a\mathbf{a} + n_b\mathbf{b} + n_c\mathbf{c} \qquad (4)$$

where n_a, n_b, and n_c are integers, and the wave vector **k** can

(23) Our calculations were carried out by employing the CAESAR and SAMOA program packages (Dai, D.; Ren, J.; Liang, W.; Whangbo, M.-H. http://chvamw.chem.ncsu.edu/).
(24) Kahn, O. *Molecular Magnetism*; VCH Publishers: Weinheim, 1993.

be written as

$$\mathbf{k} = x_a\mathbf{a}^* + x_b\mathbf{b}^* + x_c\mathbf{c}^* \quad (5)$$

where $\mathbf{a}^*$, $\mathbf{b}^*$, and $\mathbf{c}^*$ are the reciprocal vectors, and x_a, x_b, and x_c are dimensionless numbers. Then, the $\exp(i\mathbf{k}\cdot\mathbf{R})$ term of eq 3 becomes $\exp[i2\pi(x_a n_a + x_b n_b + x_c n_c)]$. It is convenient to denote $\mathbf{k}$ by showing only its dimensionless components, i.e., $\mathbf{k} = (x_a, x_b, x_c)$. The ordered magnetic state $\psi_i(\mathbf{k})$ ($i = 1-m$) is described by the linear combination of the Bloch spin functions $\sigma_\mu(\mathbf{k})$:

$$\psi_i(\mathbf{k}) = C_{1i}(\mathbf{k})\sigma_1(\mathbf{k}) + C_{2i}(\mathbf{k})\sigma_2(\mathbf{k}) + ... + C_{mi}(\mathbf{k})\sigma_m(\mathbf{k}) \quad (6)$$

The presence of up spin or down spin at a spin site μ is signified by the sign of the coefficient $C_{\mu i}(\mathbf{k})$. To determine the coefficients $C_{\mu i}(\mathbf{k})$ ($\mu = 1 - m$), we need to consider the spin exchange interaction energies $\xi_{\mu\nu}(\mathbf{k})$ between two Bloch spin functions $\sigma_\mu(\mathbf{k})$ and $\sigma_\nu(\mathbf{k})$:

$$\xi_{\mu\nu}(\mathbf{k}) = -\sum_{\mathrm{R}} J_{\mu\nu}(\mathbf{R})\exp(i\mathbf{k}\cdot\mathbf{R}) \quad (7)$$

The matrix element $\xi_{\mu\nu}(\mathbf{k})$ satisfies the relationship $\xi_{\nu\mu}(\mathbf{k}) = [\xi_{\mu\nu}(\mathbf{k})]^*$. Then, the energy $E_i(\mathbf{k})$ values associated with the ordered magnetic state $\psi_i(\mathbf{k})$ ($i = 1 - m$) are obtained by diagonalizing the interaction matrix $\Xi(\mathbf{k})$:[18,25]

$$\Xi(\mathbf{k}) = \begin{pmatrix} \xi_{11}(\mathbf{k}) & \xi_{12}(\mathbf{k}) & ... & \xi_{1m}(\mathbf{k}) \\ \xi_{21}(\mathbf{k}) & \xi_{22}(\mathbf{k}) & ... & \xi_{2m}(\mathbf{k}) \\ ... & ... & ... & ... \\ \xi_{m1}(\mathbf{k}) & \xi_{m2}(\mathbf{k}) & ... & \xi_{mm}(\mathbf{k}) \end{pmatrix} \quad (8)$$

Namely

$$\Xi(\mathbf{k})C_i(\mathbf{k}) = E_i(\mathbf{k})C_i(\mathbf{k}) \quad (9)$$

where $C_i(k)$ is the column vector of the coefficients $C_{\mu i}(k)$.

$$C_i(\mathbf{k}) = \begin{pmatrix} C_{1i}(\mathbf{k}) \\ C_{2i}(\mathbf{k}) \\ \vdots \\ C_{mi}(\mathbf{k}) \end{pmatrix} \quad (10)$$

As mentioned above, one obvious solution of eq 9 is given by $\sigma_\mu^0 = 0$ for all $\mu = 1, 2, ..., m$, which represents the completely disordered spin state at high temperatures.[18] For a given set of spin exchange parameters, one can determine the value of $\mathbf{k}$ that leads to the lowest energy, E_m, of $E_i(\mathbf{k})$ ($i = 1, 2, ..., m$), which occurs from the lowest-lying band $E_1(\mathbf{k})$. This particular $\mathbf{k}$ point may be denoted by $\mathbf{k}_m$. Then, the highest temperature T_b at which the free energy of an ordered spin state branches off from that of the disordered spin state is related to E_m as $T_b = -E_m/3k_B$,[18] and the magnetic superstructure associated with T_b is described by $\psi_1(\mathbf{k}_m)$. For instance, $\mathbf{k}_m = (0, 0, 0)$ means that the magnetic unit cell is the same as the chemical unit cell, while $\mathbf{k}_m = (1/2, 1/2, 1/2)$ means that the magnetic ordering doubles the unit cell length along each crystallographic direction.

(25) In ref 18, the symbols $\lambda_i(\mathbf{k})$ are used instead of $E_i(\mathbf{k})$.

5. Incommensurate Superstructure of $LiCuVO_4$

The spin exchange parameters of $LiCuVO_4$ (Table 1) show that the interchain NN interactions have a very weak antiferromagnetic component J_{AF}. Thus, it is not surprising that the CuO_2 chains are ferromagnetically ordered along the *a*- and *c*-directions in the magnetic superstructure (0, 0.532, 0). Thus, we will consider only the spin ordering within a single CuO_2 chain.

Consider that a CuO_2 ribbon has the repeat distance *b* and one spin site per unit cell (Figure 1a). Then, the lattice vector is given by $R = nb$ and the reciprocal vector by $\mathbf{b}^* = 2\pi/b$, and the phase factor, $\exp(i\mathbf{k}\cdot\hat{\mathbf{R}})$, of eq 3 becomes $\exp(iknb)$. Because each unit cell contains only one magnetic site, the spin exchange interaction matrix has one matrix element, i.e., $\xi_{11}(k)$. Consequently, this element itself is the magnetic interaction energy $E_1(k)$. Applying eq 7, we express $E_1(k)$: as

$$\begin{aligned} E_1(k) \equiv \xi_{11}(k) &= -J_{nn}[\exp(-ikb) + \exp(ikb)] - J_{nnn}[\exp(-i2kb) + \exp(i2kb)] \\ &= -2[J_{nn}\cos(kb) + J_{nnn}\cos(2kb)] \end{aligned} \quad (11)$$

To find the *k* value at which $E_1(k)$ has the lowest energy, we let

$$\frac{dE_1(k)}{dk} = 2b\sin(kb)[J_{nn} + 4J_{nnn}\cos(kb)] = 0 \quad (12)$$

Then, we obtain three solutions:

$$\text{at } k = 0 \qquad E_1 = -2(J_{nn} + J_{nnn}) \quad (13a)$$

$$\text{at } k = \frac{\pi}{b} \qquad E_2 = 2(J_{nn} - J_{nnn}) \quad (13b)$$

$$\text{at } k = \frac{1}{b}\arccos\left(-\frac{J_{nn}}{4J_{nnn}}\right) \qquad E_3 = \frac{J_{nn}^{\,2}}{4J_{nnn}} + 2J_{nnn} \quad (13c)$$

At $k = 0$ the phase factor $\exp(iknb)$ becomes $(1)^n$, which represents a ferromagnetic spin ordering. At $k = \pi/b$ the phase factor $\exp(iknb)$ becomes $(-1)^n$, which represents an antiferromagnetic spin ordering. When J_{nnn} is antiferromagnetic (i.e., $J_{nnn} < 0$), E_3 is lower in energy than either E_1 or E_2, and the *k* value leading to E_3 depends on the ratio of J_{nn}/J_{nnn}. Figure 8 shows a plot of the reduced wave vector, $x_b = k/\mathbf{b}^* = bk/2\pi$, versus the ratio J_{nn}/J_{nnn} according to the relationship

$$x_b = \frac{bk}{2\pi} = \frac{1}{2\pi}\arccos\left(-\frac{J_{nn}}{4J_{nnn}}\right) \quad (14)$$

The magnetic ordering that quadruples the chemical unit cell (i.e., $x_b = 0.25$) occurs when $J_{nn}/J_{nnn} = 0$, i.e., when the nearest neighbor interaction $J_{nn} = 0$ and $J_{nnn} < 0$. For $x_b = 0.25$, the phase factor $\exp(iknb)$ becomes $(i)^n$, which is $+1$,

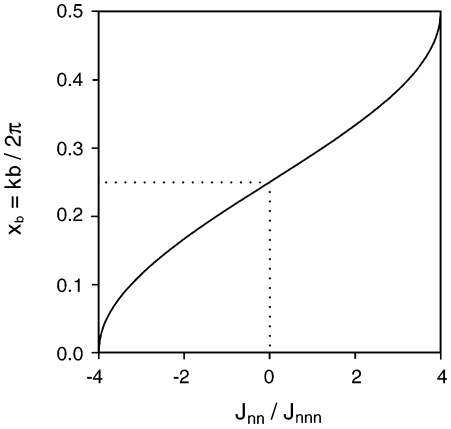

Figure 8. Wave vector associated with a LRO spin arrangement of a CuO_2 ribbon chain as a function of the J_{nn}/J_{nnn} ratio when the intrachain NNN interaction is antiferromagnetic (i.e., $J_{nnn} < 0$).

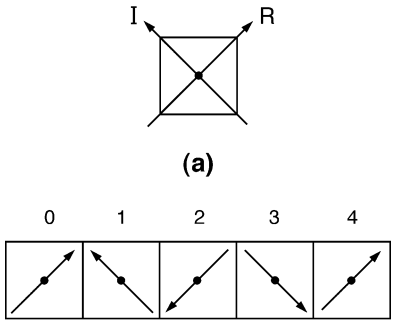

Figure 9. (a) Local complex coordinate at each CuO_4 square plane, where R and I refer to the real and imaginary axes, respectively. (b) LRO spin arrangement of a CuO_2 chain predicted when $J_{nn} = 0$ and $J_{nnn} < 0$.

i, -1, $-i$, $+1$, ..., for $n = 0$, 1, 2, 3, 4, ..., respectively. As shown in Figure 9a, the real and imaginary axes at each spin site may be chosen along the diagonal directions of the CuO_4 plane. Then, the phase factor $(i)^n$ shows that the spin vectors at the sites n spiral along the chain as depicted in Figure 9b.

Figure 8 shows that if J_{nn} is close to zero but does not vanish, the x_b value becomes $0.25 \pm \delta$, where δ is a small positive number. Then, the $1/x_b$ value becomes a noninteger number close to 4, so that the resulting magnetic superstructure becomes incommensurate with respect to the underlying chemical lattice.

6. Incommensurate and Commensurate Superstructures of CuO

The spin exchange parameters of CuO (Table 2b) show that the interchain SE interaction J_3 is much more strongly antiferromagnetic than other interchain and intrachain SE interactions, which reflects the fact that the ∠Cu−O−Cu angle is the largest for the SE path Cu(a)−O−Cu(b) (i.e., 145.8°).[17,26] Thus, the strongly interacting spin units of CuO are the one-dimensional chains $[Cu(a)-O-Cu(b)-O]_\infty$ made up of the J_3 exchange paths (hereafter referred to as the J_3-chains), as shown by the filled cylinders in Figure 5c. To a first approximation, therefore, the commensurate magnetic superstructure (0.5, 0, −0.5) of CuO that sets in below $T_{N2} = 212.5$ K can be viewed as a consequence of ordering the J_3-chains. However, this reasoning cannot answer the question why an incommensurate magnetic superstructure such as (0.506, 0, −0.483) occurs in CuO. In the following, we examine the relative strengths of J_{nn}, J_{nnn}, J_1, J_2, and J_3 needed to explain the incommensurate and commensurate superstructures of CuO on the basis of the Freiser method.

(26) Goodenough, J. B. *Magnetism and the Chemical Bond*; Wiley: Cambridge, MA, 1963.

Table 3. Pairs ($\mu-\nu$) of the Spin Sites (μ, $\nu = 1-4$) Leading to the Spin Exchange Interactions J_{nn}, J_{nnn}, J_1, J_2, and J_3

path	within a unit cell	between unit cells
J_{nn}		(1−3), (2−4)
J_{nnn}		(1−1), (2−2), (3−3), (4−4)
J_1	(1−4), (2−3)	(1−4), (2−3)
J_2	(1−2)	(1−2), (3−4)
J_3	(3−4)	(1−2), (3−4)

There are four Cu^{2+} ions per unit cell (Figure 5a, Table 2a), so that there are four spin basis functions $\sigma_\mu(\mathbf{k})$ ($\mu = 1-4$) to consider. The pairs ($\mu-\nu$) of the spin sites (μ, $\nu = 1-4$) leading to the spin exchange interactions J_{nn}, J_{nnn}, J_1, J_2, and J_3 are listed in Table 3, while the nonzero contributions to the matrix elements $\xi_{\mu\nu}(\mathbf{k})$ from the various spin exchange paths of CuO are summarized in Table 4. Thus, the nonzero matrix elements $\xi_{\mu\nu}(\mathbf{k})$ are given by

$$\xi_{11}(\mathbf{k}) = \xi_{33}(\mathbf{k}) = -2J_{nnn}\cos(2\pi x_a - 2\pi x_b)$$

$$\xi_{22}(\mathbf{k}) = \xi_{44}(\mathbf{k}) = -2J_{nnn}\cos(2\pi x_a + 2\pi x_b)$$

$$\xi_{12}(\mathbf{k}) = -J_2\{1 + \exp[-i2\pi(x_a + x_c)]\} - J_3[\exp(-i2\pi x_a) + \exp(-i2\pi x_c)]$$

$$\xi_{13}(\mathbf{k}) = -J_{nn}[\exp(-i2\pi x_a) + \exp(-i2\pi x_b)]$$

$$\xi_{14}(\mathbf{k}) = -J_1\{1 + \exp(-i2\pi x_b) + \exp(-i2\pi x_c) + \exp[-i2\pi(x_b + x_c)]\}$$

$$\xi_{23}(\mathbf{k}) = -J_1\{1 + \exp(-i2\pi x_b) + \exp(i2\pi x_c) + \exp[i2\pi(-x_b + x_c)]\}$$

$$\xi_{24}(\mathbf{k}) = -J_{nn}[\exp(i2\pi x_a) + \exp(-i2\pi x_b)]$$

$$\xi_{34}(\mathbf{k}) = -J_2[\exp(i2\pi x_a) + \exp(-i2\pi x_c)] - J_3\{1 + \exp[i2\pi(x_a - x_c)]\}$$

The $E_i(\mathbf{k})$ versus $\mathbf{k}$ plot calculated for $J_{nn} = 0$, $J_{nnn} = J_1 = J_2 = -40$ K, and $J_3 = -800$ K is shown in Figure 10a. The plot consists of two groups of dispersion curves well separated in energy. The spins of the J_3-chains are antiferromagnetically ordered in the lower-energy group but are ferromagnetically ordered in the upper-energy group. The energy separation between the two groups is solely governed by the magnitude of J_3, but the dispersion relation within each group does not depend on J_3. For the purpose of showing the dispersion relations of both groups within a plot, we take $J_3 = -200$ K without loss of generality.

The $E_i(\mathbf{k})$ versus $\mathbf{k}$ plot presented in Figure 10b shows that $\mathbf{k}_m$ does not occur around (0.5, 0, −0.5) using the J_{nn},

Table 4. Nonzero Contributions to the Matrix Elements $\xi_{\mu\nu}(\mathbf{k})$ from the Spin Exchange Paths between the Spin Sites μ and ν (μ, $\nu = 1-4$) of CuO[a]

μ	ν	cell	Cu···Cu	contribution to $\xi_{\mu\nu}(\mathbf{k})$
1	1	[1, 1, 0]	5.801	$-J_{nnn}\exp[i2\pi(-x_a + x_b)]$
		[1, −1, 0]	5.801	$-J_{nnn}\exp[i2\pi(x_a - x_b)]$
1	2	[−1, 0, −1]	3.173	$-J_2\exp[-i2\pi(x_a + x_c)]$
		[0, 0, 0]	3.173	$-J_2$
		[−1, 0, 0]	3.748	$-J_3\exp(-i2\pi x_a)$
		[0, 0, −1]	3.748	$-J_3\exp(-i2\pi x_c)$
1	3	[−1, 0, 0]	2.900	$-J_{nn}\exp(-i2\pi x_a)$
		[0, −1, 0]	2.900	$-J_{nn}\exp(-i2\pi x_b)$
1	4	[0, −1, −1]	3.083	$-J_1\exp[-i2\pi(x_b + x_c)]$
		[0, −1, 0]	3.083	$-J_1\exp(-i2\pi x_b)$
		[0, 0, −1]	3.083	$-J_1\exp(-i2\pi x_c)$
		[0, 0, 0]	3.083	$-J_1$
2	2	[−1, −1, 0]	5.081	$-J_{nnn}\exp[-i2\pi(x_a + x_b)]$
		[1, 1, 0]	5.081	$-J_{nnn}\exp[i2\pi(x_a + x_b)]$
2	3	[0, −1, 1]	3.083	$-J_1\exp[i2\pi(-x_b + x_c)]$
		[0, −1, 0]	3.083	$-J_1\exp(-i2\pi x_b)$
		[0, 0, −1]	3.083	$-J_1\exp(-i2\pi x_c)$
		[0, 0, 0]	3.083	$-J_1$
2	4	[1, 0, 0]	2.900	$-J_{nn}\exp(i2\pi x_a)$
		[0, −1, 0]	2.900	$-J_{nn}\exp(-i2\pi x_b)$
3	4	[0, 0, −1]	3.173	$-J_2\exp(-i2\pi x_c)$
		[1, 0, 0]	3.173	$-J_2\exp(i2\pi x_a)$
		[0, 0, 0]	3.748	$-J_3$
		[1, 0, −1]	3.748	$-J_3\exp[i2\pi(x_a - x_c)]$

[a] The spin pair (3−3) is equivalent to (1−1), and the spin pair (4−4) is equivalent to (2−2).

J_{nnn}, J_1, J_2, and J_3 parameters listed in Table 2b. To find a condition necessary for $\mathbf{k}_m$ to occur around (0.5, 0, −0.5), we varied the values of J_1 and J_2 while keeping $J_{nn} = 0$, $J_{nnn} = -40$ K, and $J_3 = -200$ K. As shown in Figure 10c−e, $\mathbf{k}_m$ occurs around (0.5, 0, −0.5) if J_2 is weakly ferromagnetic and if J_1 is weakly antiferromagnetic.

Figure 10e shows that $\mathbf{k}_m$ becomes (0.5, 0, −0.5) only if $J_1 = 0$, i.e., only if the spin ordering along the [Cu(a)−O−Cu(e)−O]$_\infty$ chain (Figure 5c) has no influence on the stability of the spin arrangement. In the LRO spin arrangement given by the point $\mathbf{k} = (0.5, 0, -0.5)$, each [Cu(a)−O−Cu(b)−O]$_\infty$ chain has an antiferromagnetic arrangement as expected, and each [Cu(a)−O−Cu(c)−O]$_\infty$ chain (i.e., the CuO_2 ribbon chain) has an (↑↑↓↓)$_\infty$ spin arrangement as found for the CuO_2 chains in $LiCuVO_4$.[17] In addition, each [Cu(a)−O−Cu(d)−O]$_\infty$ chain has a ferromagnetic spin arrangement while each [Cu(a)−O−Cu(e)−O]$_\infty$ chain has an (↑↑↓↓)$_\infty$ spin arrangement.[17]

Figure 10c,d shows that $\mathbf{k}_m$ becomes incommensurate ($0.5 + \delta$, 0, $-0.5 + \epsilon$), where δ and ϵ are small positive numbers, if J_1 is negative but close to zero. Our calculations show that for $J_{nn} = 0$, $J_{nnn} = -40$ K, $J_2 = 20$ K, and $J_3 = -200$ K, $\mathbf{k}_m$ becomes (0.508, 0, −0.483) when $J_1 \approx -3.6$ K. This incommensurate value is quite close to the observed incommensurate super structure (0.506, 0, −0.483). It is important to note that the incommensurate superstructure becomes commensurate by a small change in J_1 from −3.6 K to 0. This finding is consistent with the experimental observation that the incommensurate structure becomes commensurate by a slight lowering of the temperature (from 231 to 212.5 K).[7b] It is most likely that the temperature lowering induces a slight change in the crystal structure, which in turn makes the weak antiferromagnetic interaction J_1 vanish.

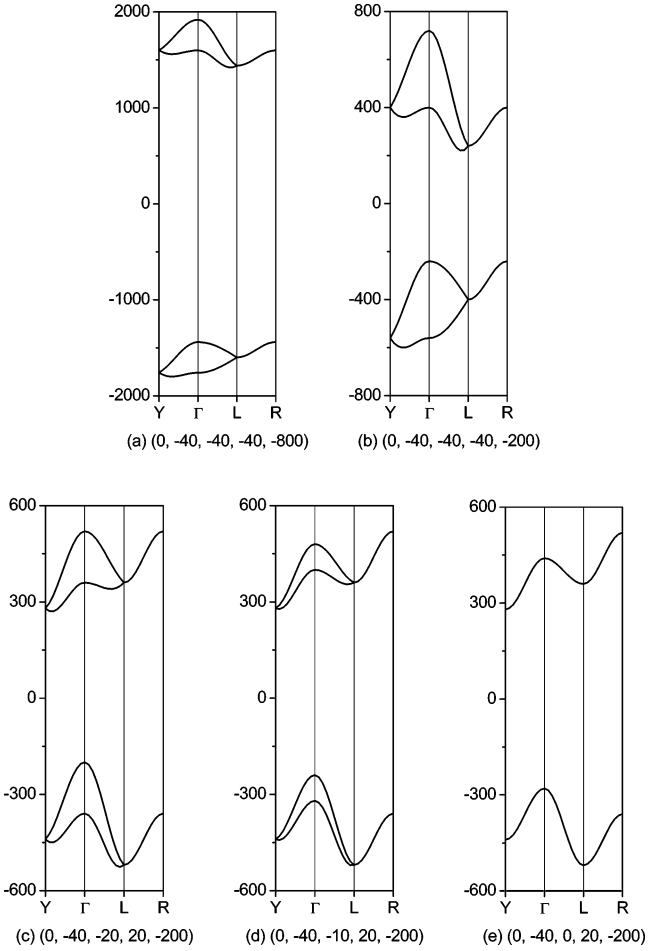

Figure 10. Dispersion relations of the magnetic energy levels calculated for CuO for various sets of spin exchange parameters (J_{nn}, J_{nnn}, J_1, J_2, J_3). The values of the exchange parameters and the magnetic energy are given in units of K. In terms of the reciprocal vectors **a***, **b***, and **c***, the wave vector points are given by $\mathbf{\Gamma} = (0, 0, 0)$, $\mathbf{Y} = (0, 0.5\mathbf{b}^*, 0)$, $\mathbf{L} = (0.5\mathbf{a}^*, 0, 0.5\mathbf{c}^*)$, and $\mathbf{R} = (0.5\mathbf{a}^*, 0.5\mathbf{b}^*, 0.5\mathbf{c}^*)$.

7. Discussion

The relative strengths of the spin exchange parameters needed to explain the magnetic superstructures of CuO using the Freiser method deviate somewhat from those estimated on the basis of spin dimer analysis by calculating $(\Delta e)^2$. It should be recalled that the spin exchange parameters estimated from $(\Delta e)^2$ values refer to the antiferromagnetic terms J_{AF}, because the ferromagnetic terms J_F were ignored in this analysis. It is important to have a rough estimate of J_F to see whether the spin exchange parameters required by the Freiser method to explain the magnetic superstructures of $LiCuVO_4$ and CuO are reasonable.

Each CuO_2 chain of $LiCuVO_4$ has two Cu^{2+} ions per chemical unit cell. Since its superstructure (0, 0.532, 0) is equivalent to the superstructure (0, 0.468, 0), the x_a value of the CuO_2 chains leading to the observed superstructure is either 0.266 or 0.234 if each CuO_2 chain were regarded as having one Cu^{2+} ion per chemical unit cell. Then, the use of $x_a = 0.266$ and 0.234 in eq 14 leads to $J_{nn}/J_{nnn} = 0.40$ and −0.40, respectively. Given that $J_{nnn} = -45$ K, the J_{nn} value can be either −18 or 18 K. However, the choice of $J_{nn} = 18$ K is correct because the J_{AF} contribution to J_{nn} is

Table 5. Spin Exchange Parameters J_{nn} and J_{nnn} Estimated for the CuO_2 Ribbon Chain of Li_2CuO_2

	J_{nn}/k_B (K)	J_{nnn}/k_B (K)
this work[a]	−4.3	−53
first principles[b]	100	−62
first principles[c]	142	−22
neutron scattering[d]	−2.8	1.9

[a] The J_{AF} values are based on the $(\Delta e)^2$ values. [b] Reference 27. [c] Reference 28. [d] Reference 29.

Table 6. Comparison of the Geometrical Parameters Associated with the Spin Exchange Paths J_{nn} and J_{nnn} in $LiCuVO_4$, Li_2CuO_2, and CuO[a]

	$LiCuVO_4$[b]	Li_2CuO_2[c]	CuO[d]
(a) Cu−O−Cu Path J_{nn}			
Cu−O	1.951	1.958	1.961
O−Cu	1.951	1.958	1.951
∠Cu−O−Cu	96.0	94.0	95.7
(b) Cu−O···O−Cu Path J_{nnn}			
Cu−O	1.951	1.958	1.961
O···O	2.900	2.863	2.901
O−Cu	1.951	1.958	1.951
∠Cu−O···O	138.0	137.0	138.0
∠O···O−Cu	138.0	137.0	137.7

[a] The lengths and angles are in angstrom and degree units, respectively. [b] Reference 1. [c] Reference 2. [d] Reference 3.

weak (i.e., −4 K, Table 1) and because the J_F value is positive. As already pointed out, the repulsion integral K_{12} ($= J_F/2$) of an SE interaction originates mainly from the O 2p-orbital tails residing on the same bridging oxygen atoms. The J_{nn} interaction has two Cu−O−Cu superexchange paths. Consequently, from $J_{nn} = 18$ K and $J_{AF} = -4$ K, the J_F value per Cu−O−Cu path is estimated to be about 11 K.

A much greater estimate of J_F is obtained by considering the spin exchange interactions of Li_2CuO_2 which consists of isolated CuO_2 ribbon chains. Table 5 lists the J_{nn} and J_{nnn} values of its CuO_2 chain calculated by first principles electronic structure calculations[27,28] as well as the corresponding values from the present spin dimer analysis. Our estimate for the SSE path J_{nnn} is comparable to those from the first principles calculations. The SE path J_{nn} is estimated to be strongly ferromagnetic by the first principles calculations. Our estimate shows that the contribution of the J_{AF} term to J_{nn} is negligible, so that the J_{nn} values estimated from first principles calculations may be interpreted as reflecting mainly the J_F values. Then, the J_{nn} value of 100−140 K obtained from the first principles suggests the J_F value of 50−70 K per Cu−O−Cu path. This value of J_F would be an overestimate because the geometrical parameters of the J_{nn} and J_{nnn} paths of Li_2CuO_2 are very close to those of $LiCuVO_4$ (Table 6).

It should also be pointed out that the spin wave of Li_2CuO_2 observed at 1.5 K from a neutron scattering study[29] presents quite a different picture in terms of both the signs and the magnitudes of J_{nn} and J_{nnn} (Table 5). According to this study, the interchain SSE path J_{ac} along the $(a + c)$-direction has the strongest antiferromagnetic interaction (i.e., $J_{ac} = -4.5$ K). The latter implies that the magnetic orbitals representing the two spin sites of a spin dimer overlap more strongly in the J_{ac} path than in the J_{nnn} path. The latter is highly unlikely, given that the two magnetic orbitals representing the Cu^{2+} spin sites are not coplanar in the J_{ac} path but are coplanar in the J_{nnn} path. It is desirable to determine the magnetic structure of Li_2CuO_2 by neutron diffraction measurements.

Our analysis of $LiCuVO_4$ using the Freiser method shows that its magnetic superstructure originates essentially from the tendency for each CuO_2 chain to have their spins order antiferromagnetically. This tendency arises from the fact that $J_{nnn} < 0$, $J_{nn} > 0$, and $J_{nn} \ll |J_{nnn}|$. Our estimates of the spin exchange parameters are in agreement with this conclusion. The incommensurate superstructure of $LiCuVO_4$ originates from the fact that the NN interaction J_{nn} is nonzero.

The three interchain SE interactions J_1, J_2, and J_3 of CuO ($J_{AF} = -46$, −55, and −870 K, respectively, Table 2b) each have one Cu−O−Cu path. According to the above estimate of J_F, the J_1 and J_2 interactions could become either weakly ferromagnetic or weakly antiferromagnetic, whereas the J_3 interaction should remain strongly antiferromagnetic (i.e., in the range of −800 K). The latter estimate is in good agreement of the J_3 value, -780 ± 233 K, deduced from the neutron scattering study.[7b] Both the incommensurate superstructure (0.506, 0, −0.483) and the commensurate superstructure (0.5, 0, −0.5) of CuO are explained in terms of the total spin exchange interaction energies calculated by the Freiser method. The conversion of the incommensurate to the commensurate superstructure requires only a slight change in the interchain interaction J_1 from −3.6 K to 0. The latter is fully consistent with the experimental observation that the incommensurate structure becomes commensurate by a slight lowering of the temperature (from 231 to 212.5 K).[7b]

8. Concluding Remarks

The magnetic superstructure of $LiCuVO_4$ below 2.1 K shows that the NNN spins are antiferromagnetically coupled in each chain, and hence, the NNN spin exchange interaction J_{nnn} is more strongly antiferromagnetic than the NN spin exchange interaction J_{nn}. Thus, the intrachain spin exchange parameter of −45 K, deduced from the magnetic susceptibility of $LiCuVO_4$, should be assigned to J_{nnn}. The magnetic superstructure of $LiCuVO_4$ is largely driven by the tendency for each CuO_2 chain to have their NNN spins order antiferromagnetically. Our classical spin analysis of $LiCuVO_4$ using the Freiser method shows that the incommensurate superstructure originates from nonzero J_{nn}, and that the observed incommensurate superstructure means $J_{nn}/J_{nnn} = -0.40$. The latter leads to the estimate $J_{nn} = 18$ K. The incommensurate superstructure (0.506, 0, −0.483) of CuO is explained by the Freiser method, if J_2 is weakly ferromagnetic and if J_1 is weakly antiferromagnetic. The conver-

(27) Mizuno, Y.; Tohyama, T.; Maekawa, S.; Osafune, T.; Motoyama, N.; Eisaki, H.; Uchida, S. *Phys. Rev. B* **1998**, *57*, 5326.
(28) de Graaf, C.; Moreira, I. de P. R.; Illas, F.; Iglesias, O.; Labarta, A. *Phys. Rev. B* **2002**, *66*, 14448.
(29) Boehm, M.; Coad, S.; Roessli, B.; Zheludev, A.; Zolliker, M.; Böni, P.; Paul, D. M.; Eisaki, H.; Motoyama, N.; Uchida, S. *Europhys. Lett.* **1998**, *43*, 77.

sion from the incommensurate structure to the commensurate superstructure (0.5, 0, −0.5) requires a slight change in the interchain interaction J_1 (from −3.6 K to 0), in harmony with the experimental finding that the incommensurate structure becomes commensurate by a slight lowering of the temperature. The present work suggests that the Freiser method is indispensable in understanding incommensurate and commensurate magnetic superstructures of magnetic solids, when used in conjunction with the spin exchange parameters estimated from an appropriate spin dimer analysis.

Acknowledgment. This work was supported by the Office of Basic Energy Sciences, Division of Materials Sciences, U.S. Department of Energy, under Grant DE-FG02-86ER45259. M.-H.W. thanks Dr. Reinhard K. Kremer (Max-Planck-Institut für Festkörperforschung, Stuttgart) for invaluable discussion and for making available his neutron diffraction and magnetic susceptibility results of $LiCuVO_4$ prior to publication.

IC035314C